Preface: Focus on imaging methods in granular physics

Axelle Amon, Philip Born, Karen E. Daniels, Joshua A. Dijksman, Kai Huang, David Parker, Matthias Schröter, Ralf Stannarius, and Andreas Wierschem

---

Preface: Focus on imaging methods in granular physics

Axelle Amon,[1] Philip Born,[2] Karen E. Daniels,[3] Joshua A. Dijksman,[4] Kai Huang,[5]
David Parker,[6] Matthias Schröter,[7] Ralf Stannarius,[8] and Andreas Wierschem[9]

[1]*Institut de Physique de Rennes, UMR UR1-CNRS 6251, Université de Rennes 1, 35042 Rennes, France*
[2]*Institut für Materialphysik im Weltraum, Deutsches Zentrum für Luft- und Raumfahrt, 51170 Cologne, Germany*
[3]*Department of Physics, North Carolina State University, Raleigh, North Carolina 27695, USA*
[4]*Physical Chemistry and Soft Matter, Wageningen University and Research, Wageningen, The Netherlands*
[5]*Experimentalphysik V, Universität Bayreuth, 95440 Bayreuth, Germany*
[6]*School of Physics and Astronomy, University of Birmingham, Birmingham B15 2TT, United Kingdom*
[7]*Institute for Multiscale Simulation, Friedrich-Alexander-Universität Erlangen-Nürnberg (FAU),
91052 Erlangen, Germany*
[8]*Institut für Experimentelle Physik, Otto-von-Guericke-Universität, 39106 Magdeburg, Germany*
[9]*Institute of Fluid Mechanics, Friedrich-Alexander-Universität Erlangen-Nürnberg (FAU), 91058 Erlangen,
Germany*

I. CURRENT CHALLENGES

To see a world in a grain of sand, and a heaven in a wild flower.

The poem *Auguries of Innocence* by William Blake illustrates one of the complexities of granular physics: Each grain of sand is unique[1] and the entirety of particle-particle interactions in a sand pile is unpredictable.[2] While walking on a beach, one intermittently experiences the transition between a rigid, solid-like state and a fluid-like state. One leaves behind the stress loading history in the form of footprints.[3,4] Stepping into the water, one recognizes the sediments are looser in comparison to the partially wet sand on the beach and susceptible to the surrounding fluid flow, leading to sand ripples.[5]

Continuum descriptions based on empirical assumptions can successfully describe rapid flows and sufficiently dilute granular gases.[6–8] However, continuum approaches fail to describe slow dense flows or critical behavior such as intermittent flows, jamming, and pattern formation.[9,10] These systems are governed by phenomena which are hard to model in continuum descriptions: strong dissipation at the contacts between the grains due to friction,[11] inelastic deformation,[12] and cohesion,[13] etc. Moreover, the athermal nature of the system does not allow for the use of statistical physics to connect the micro-scale to the macro-scale.

One of the major issues in modeling granular materials arises from the fact that what happens at the scale of a single grain can impact the response of the whole material. In static piles and dense flows, the distribution of stress is governed by force chains.[14] Those force chains sensitively depend on the individual contacts between the grains, and the history of loading those contacts.[15,16] Consequently, local properties of the contacts, such as their typical orientation or the nature of the frictional contacts, can modify the mechanical behavior of the system. For example, anisotropy in the orientation of those contacts,[17] arising due to shear, can have a major impact on the macroscopic response.

On an intermediate scale between the size of the grains and the sample as a whole, it has been shown that the non-affine motion of the system, at the scale of clusters of typically ten grains, plays a non-negligible role in the mechanical response of the system.[18] This non-affine motion seems to control numerous features of amorphous materials such as the thickness of shear bands[19] or the eddy-like structures in dense flows.[18] Several nonlocal effects have been observed, particularly in confined flows. For example, it has been demonstrated that shear bands generate mechanical noise even deep into the seemingly static phase.[20,21]

Therefore, it is of paramount importance for a description of granular matter to be able to make observations on many length scales: from the grain or contact scale, through the mesoscopic effects such as nonlocality and shear banding, which appear on the ~10 grain scale, even up to the scale of a full sample that may contain billions of grains.

At the grain scale, there are two generic issues making it difficult to extract data with any imaging technique. First, our most advanced imaging technologies have been developed to act as extensions for our eyes, which operate in the visible spectrum. However, most granular materials are opaque in this range of wavelengths. Even if the particles were transparent, their refractive index would not generically match that of the most common interstitial fluids (air or water), leading to multiple scattering. Second, a large volume of raw data is required to analyze a complete granular system: even just a simple sugar cube contains on the order of 10^5 individual grains. To identify the center of mass and orientation of each of these grains, it is necessary to identify its spatial extent using several thousand voxels (3D pixels). As a consequence, several gigabytes of data need to be collected to analyze a single static packing of grains. Moreover, trying to describe any kind of dynamics will compound the problem by requiring a sufficiently high frame rate to collect those data.

There are a number of ways to address the opacity issue, even with visible light. A common technique is to perform quasi-two-dimensional (Q2D) experiments, allowing the complete tracking of particle positions[22,23] as well as the particle-particle interactions.[24] Another option is to restrict the data

collection to the surface of the granular system, with the disadvantage that bulk properties can differ significantly from the behavior at the surface.[25–30] If the volume fraction of the particles is sufficiently low, stereo-camera or volumetric methods can be used to capture three-dimensional (3D) dynamics.[31–33] If the particles are optically transparent, there exist two additional options. Where the interstitial liquid can be chosen freely, index matching provides a means to acquire 3D data.[34] Alternatively, it is possible to embrace the multiple scattering effects and use coherent light to gather information from the resulting speckle pattern.[35] Finally, we can abandon the range of visible light entirely and instead use penetrating radiation to obtain the data from the bulk of the sample. A variety of such methods are extensively covered in this focus edition, covering terahertz electromagnetic radiation,[36] radar,[37] positron emission,[38] nuclear magnetic resonance,[39] and X-ray tomography.[40]

Several solutions also exist for the data-bandwidth issue, which are common to the various methods. Limiting the analysis to 2D or the surface of a 3D system is an effective way to decrease the number of particles under analysis, at the expense of ignoring the bulk behavior. To access the bulk, it is possible to restrict the analysis to quasi-static systems in which the driving is stopped during each cycle to take a snapshot. This will reduce the necessary frame rate to zero, eliminating problems with bandwidth. Alternatively, the experiment can be constructed so that only a subset of tracer particles is visible to the image acquisition system, or to take depth-averaged signals, in order to retain the dynamics.

The present focus issue mainly covers imaging with electromagnetic waves. Nevertheless, acoustic waves can also be used to measure local velocities of particles in dilute flows[41,42] or elastic properties of the effective medium for dense systems.[43] A problem is that multiple scattering prevents spatial resolution with acoustic waves in dense granular piles. Another difficulty when using acoustic waves is the intrusiveness of the probe that acts at the level of the contacts between the grains.

This overview article, as well as the following focus issue on imaging granular particles, aims to provide guidance and orientation concerning the experimental techniques which help to face all these challenges.

II. ACQUIRING PARTICLE POSITIONS, ORIENTATIONS, AND SHAPES

To acquire particle positions, orientations, and shapes, a two-step process is necessary. First, an image is made of a particle and its immediate surroundings. Second, the required particle information is extracted through data analysis of those images. For both steps, there are multiple methods to chose from (Table I); in this Focus Issue, we discuss both steps in some detail.

To image a particle, some contrast between the particle and its surrounding medium is required. The most obvious method to detect particles is to use the visible part of the electromagnetic spectrum. In this range, it suffices to use standard cameras to obtain digital images of a collection of particles. The only difference between 2D and 3D imaging is whether each configuration is represented as a single 2D image or as a stack of 2D slices. Due to both absorption and scatter, however, the visible spectrum has limited penetration into most materials. Since the time of the first packing experiments by Bernal,[45] one solution has been to create 3D images by physically disassembling the packing and taking an image at each step. This method is still used in the present day for sufficiently slow flows.[46]

To avoid such destructive methods, and considerably improve the data collection rate, modern experiments commonly use transparent granular media. For optical transmission through a pile of transparent glass marbles, however, scatter remains a significant limitation in going deeper than a few particles inward from the boundary. The solution is to reduce the scatter by immersing the solid particles in an index-matched medium. To obtain the necessary image contrast, at least one of the two phases must be stained with a fluorescent dye. Thus, by illuminating a cross section of the medium with a sheet of light (usually via a laser), the fluorescent response of the dyed material within the sheet is captured by the camera. By moving the light sheet with respect to the sample and recording a series of slices, a 3D image of the medium can be created.

In the resulting 3D image, computerized-post processing algorithms can then be used to track particles, measure flow velocities, or identify shapes. This technique of Refractive Index Matched Scanning (RIMS) has been covered by several review articles.[47,48] The RIMS article in this Focus Issue will explore the application of RIMS[34] to hydrogel particles in particular. These are soft elastic solids with a refractive index close to that of water. The softness of hydrogels provides a key feature: they deform significantly under modest loads. The presence of deformations at each contact makes it possible to quantify individual contact forces on hydrogels, as is discussed in Sec. IV. The central challenge is to find the nonspherical contour of the particle. An example can be seen in Fig. 1(a).

TABLE I. Techniques for obtaining particle coordinates, typical values.

| Technique	2D/3D	Spatial resolution	Maximal framerate	Range of materials	Comments
Disassembly, excavation	3D	Better than particle size	1 per h	Practically all	Destructive
Index-matching (RIMS)	2D and 3D	10 μm/voxel	1 per min	Transparent	
MRI	2D and 3D	$\approx$100 μm/voxel	10 per sec.	Liquids containing ^{1}H	
Optical imaging	2D	1 μm/pixel	10 per ms	Broad	
X-ray tomo (X-ray tube)	3D	1 μm/voxel	1 per 10 min.	Broad	
X-ray tomo (synchrotron)	3D	1 μm/voxel	5 per s	Broad	Small FOV
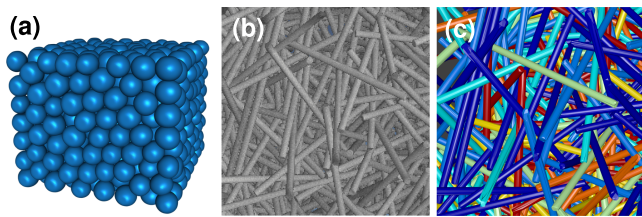
FIG. 1. 3D imaging of granular particles. (a) Compressed hydrogel spheres with 2 cm diameter (Educational Innovations), imaged by laser sheet scanning in an index-matched liquid. Particle deformations in a compressed packing of soft spheres are clearly visible, for example, in the flattening of spheres at the top. Such deformations are measurable at each particle-particle contact and yield information about contact forces. (b) Rendering of the volume data obtained by X-ray tomography, the particles are cylinders with 40 mm length and 1.4 mm diameter (Spaghettini Barilla N. 3). An animated version of similar raw data can be found at Ref. 44. (c) Rendering of the same volume as in the last panel, but after the detection of all cylinder positions and orientations. The particles are color coded with their contact number. Images b and c by courtesy of Cyprian Lewandowski.

For non-transparent materials, Magnetic Resonance Imaging (MRI) can obtain contrast-rich images within the bulk.[39] MRI reveals the edges of particles by mapping the distribution of NMR-active nuclei in liquids (or, in exceptional cases also in gases) within a sample. Two requirements have to be met. First, it is necessary to have a liquid constituent within the sample, since solids typically do not yield useful MRI signals. Second, the liquid needs to have NMR-active nuclei. There are a large number of NMR-active isotopes. While phosphorus, fluorine, or ^{13}C enriched carbon would work in principle, in practice all commercial MRI scanners work at the proton resonance frequency, i.e., they are tuned to detect the ^{1}H nuclei in the sample. For this reason, the most common methods for achieving contrast are to use water- or oil-containing particles (e.g., seeds or synthetic capsules) or to coat/embed solid particles in a hydrogen-containing fluid. In these cases, a conventional tomograph can achieve submillimeter spatial resolution. Samples of several dozen centimeters can be handled by large MRI tomographs, medical scanners, or wide-bore scanners.

Just as for RIMS, MRI can provide a 3D image or *tomogram* of a sample, from which particle orientations and shapes may be retrieved. In some situations, it suffices to record a single 2D slice of the sample in order to track the dynamics. If so, both RIMS and MRI can provide single slices at a faster data-collection rate (kHZ).

Another technique we discuss in this Focus Issue is X-ray tomography.[40] Its advantages are superior spatial resolution and the ability to work with a much more diverse set of materials, including even pasta (see Figs. 1(b) and 1(c)). In contrast to visible light, X-rays will penetrate most granular samples with an intensity that decays exponentially with distance into the material. For a broad range of materials, the X-ray contrast is large enough to provide images. A major drawback is that the acquisition of even a simple cross-sectional view in general requires the same amount of time as the full 3D image. This makes the technique comparatively slow. A compromise is to take 2D transmission images (radiograms) by placing the granular sample between an X-ray source and a camera equipped with a scintillator. In this case, the X-ray signal is integrated across the full sample.

In computed tomography (CT), a large number (typically $\sqrt{2}$ times the width of the image in pixels) of radiograms are collected while rotating the sample around an axis perpendicular to the beam direction. From this sequence of images, a 3D representation of the sample is reconstructed using an algorithm called the inverse Radon transformation.[49] Each voxel represents the X-ray absorption coefficient within a volume element at the corresponding location in the sample. Since different materials have different absorption coefficients, this information can serve as the contrast to detect the boundaries of particles and thus allows identifying the position, shape, and orientation of all granular particles within the tomogram.[40]

The time needed to acquire an X-ray tomogram depends on the photon flux from the source. There are two types of sources: classical X-ray tubes and synchrotrons. X-ray tubes are comparatively low cost, allowing the production of turnkey, tabletop tomography setups with resolutions down to the submicron range. Such setups can even be assembled by scientists themselves.[50] However, X-ray tubes provide a low photon flux and thus require 10 min to several hours to generate a single 3D image. Synchrotrons are several orders of magnitude brighter than X-ray tubes, thus allowing the acquisition of tomograms at rates up to several per second. However, because they are large user facilities, they require significant lead time starting with an application for beam time. Moreover, their field of view (FOV) is typically limited to less than a cubic centimeter.

All of the imaging methods discussed above provide a 2D or 3D image of a granular sample. The algorithmic analysis steps required to quantify particle properties from such images are in principle generic and can in many cases be applied to images of any imaging method. However, since every imaging method comes with its own specific noise and artifacts, an algorithmic analysis of image data usually begins with a method-dependent step for denoising and removing artifacts.

Even with perfect image denoising and artifact removal, there remain significant fundamental challenges in image analysis. A denoised image will be a 2D or 3D set of gray values. The gray value of each pixel/voxel can variously represent the amount of directly reflected light, the concentration of excited fluorescent dye, a density of spins, or an X-ray absorption coefficient. This could be measured for either the particle or for its surrounding medium. Either way, the number of pixels/voxels is limited, and the gray values are drawn from a bounded set of integers. Thus, both the spatial resolution and the image contrast gradients are always finite. This limitation yields a fuzziness on the precise contour of every imaged particle. This is especially detrimental in images of dense particulate media: the fuzziness limits our ability to recognize where particles are exactly located, whether two neighboring objects are touching, or even whether they are in fact separate entities.

A natural first technique is to simply apply a gray value threshold, but this is often insufficient for separation and identification of particles. Instead, an extensive number of algorithms have been developed, often with a significant input from the field of computer science, which allow for distinguishing particles both from the background and from each other.[40] In

addition, there are a number of post-processing methods to detect the location of a particle surface, for which the shape does not have to be known *a priori*.[34,51]

After the extraction of detailed shape information about the location of the outer boundary of each particle, further analysis of the experimental data becomes possible. Common techniques include examining nearest neighbor distributions,[40] particle tracking and velocimetry (see Sec. III), contact force measurements (see Sec. IV), and more intricate measures that characterize the packing structure, such as Minkowski tensors.[40]

III. MEASURING PARTICLE DISPLACEMENTS AND VELOCITIES

Measuring velocities starts with first measuring the displacements of objects or patterns between two snapshots separated by a time interval. These measurements can then be accumulated into either a velocity field (for a Eulerian viewpoint) or particle-trajectories (Lagrangian viewpoint), according to the needs of the researcher.

In making displacement measurements, two fundamental limitations must be considered. First, the precision with which the position of the objects is known, to be improved according to the techniques described in Section II. Second, what choice of frame rate can be obtained using the chosen particle-finding method, and whether this time scale is sufficiently well-separated from the dynamics of interest. Several key sources of error inherent in these choices are reviewed in Ref. 52.

The frame rate depends on parameters such as the desired resolution (number of pixels/voxels) and the exposure time needed for a sufficient signal-to-noise ratio. Depending on the specific questions of interest, different experimental strategies can be chosen. Innovative methods are often custom-designed for a particular situation. Performance indicators of the different displacement/velocity methods discussed in this Focus Issue are summarized in Table II.

A straightforward method for obtaining the Lagrangian trajectories of well-identified particles is to start from a temporal sequence of their successive positions, and from these deduce their full velocities. High-precision particle position measurements play a key role in the success of this method, and identifying single particles is not trivial on its own. One way to track individual particles is to tag a small number of tracers

which can be easily distinguished. This can be done with either one or several cameras, to increase spatial or dimensional coverage. Tracking the centers of the particles is sufficient for studying translational motion. Rolling or sliding particle motion can be identified only by taking into account further characteristics of the extended particle, like form, intensity distribution, tracking marks or patterns on the particles, which will be discussed further in an article of this Focus Issue.[53]

For particles which are opaque or not index-matched with the surrounding media, velocity measurements are restricted to near-surface flows or to low particle concentrations. Refractive-index matching between fluid and particles allows the study of deeper layers in granular matter, a technique discussed in one of the articles of the Focus Issue.[34] Other techniques for tracking within the bulk include Positron Emission Particle Tracking (PEPT),[38] microwave radar tracking,[37] X-ray radiography,[54] or Magnetic Resonance Imaging (MRI).[39] Tracer particles (single radioactively labeled in the case of PEPT, high dielectric constant for radar tracking, steel spheres for X-ray radiography, or NMR-active nuclei for MRI) are then embedded inside the material (or spin-labeled in MRI) and the system is imaged while subjected to some excitation or loading. The knowledge of the complete trajectory of one or a few particles in 3D is then possible. In such methods, slow frame rates are not an impediment to the tracking of particles as the particles are well-separated in space. In the case of MRI, magnetization relaxation of labeled tracers may limit the total duration of the dynamics studied. Using PEPT[38] a single particle can be followed almost indefinitely, and a well-mixed system can provide representative information on the entire phase space of this type of particle. In other systems, the trajectory of a single tracer is not always a representative of the whole velocity field, so that full-field methods are preferred.

In order to follow an assembly of indistinguishable grains, particle tracking velocimetry (PTV) can be achieved by matching particle positions across sequential images.[55–57] To discriminate identical particles in subsequent images, the displacement must be smaller than typically half of the spacing between particle centers, which requires that the frame rate is sufficiently large compared to the dynamics of the particles.[52] For particle-matching between different frames, various algorithms can be employed. The principle behind tracking algorithms is shown in Figure 2(a) and an example of a displacement field obtained using PTV is shown in Figure 2(b). An important issue is obtaining sufficiently accurate positions

TABLE II. Techniques for obtaining particle velocities and displacements.

| Technique	2D/3D	Tracer/ all part.	Maximal framerate	Range of materials
DWS	(2 + 1/2)D	All	Limited by the photon flux at high frame rate	Multiple scattering, low absorption
Index-matching (RIMS)	2D and 3D	Tracer or all	O(10 kHz) (tracer); 1/min (all)	Transparent
MRI	2D and 3D	Tracers or all	≈10/s	Only liquids containing ^{1}H
PEPT	3D	Tracer	O(kHz)	Any
PIV	2D, (2 + 1)D, 3D	All	Interframe time: O(100 ns)	Broad
Radar	3D	Tracer	Operating frequency, O(GHz)	Contrast of dielectric constant
Time-resolved PIV	2D	All	O(10 kHz)	Broad
X-ray radiograms	2D	Tracer	100 Hz (X-ray tube)	Density contrast
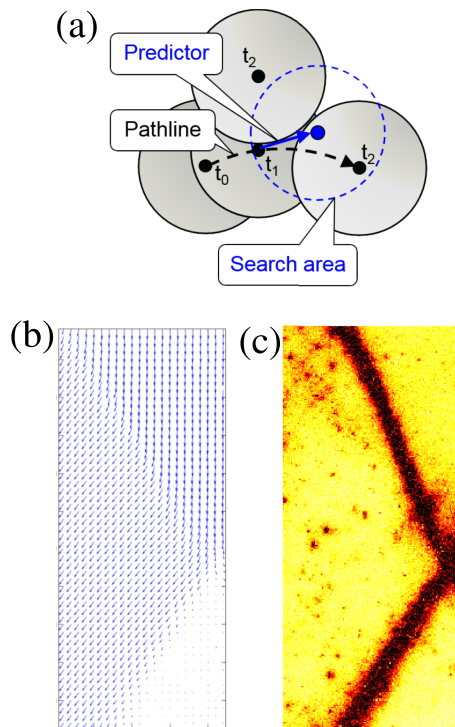
FIG. 2. (a) Sketch for particle matching in PTV using a predictor from previous displacement. This method allows a more accurate tracking of the particles than a mere nearest-neighbor algorithm. The same displacement field obtained by two different methods ((b) and (c)) during a biaxial test after the failure of the material. (b) Displacement field obtained by tracking the reflection of the glass beads at the surface of the sample (PTV). (c) Deformation field obtained by computing correlation between two successive speckle images obtained from the coherent light backscattered by the material (DWS). Yellow: low deformation ($\lesssim 10^{-5}$), black: large deformation ($\gtrsim 10^{-4}$). A description of the experiment and results can be found in Ref. 35.

to identify displacements, while still operating at high enough frame to capture the dynamics. This trade-off is made differently for different systems. In general, 3D scans are used for studying slower dynamics, while fast dynamics require fast cameras aimed at a single slice of the material or a Q2D system.

Where it is not possible to identify individual particles, it is still possible to measure mean displacements (or velocity/deformation fields) using cross correlation techniques like particle image velocimetry (PIV).[31–33] These techniques work by subdividing individual frames into small interrogation areas. For these areas, the mean displacement is determined by cross correlation between subsequent frames. A sub-pixel resolution can be achieved by an appropriate choice of imaging conditions and the size of the interrogation area. Using more than one camera, stereoscopic or volumetric studies can be carried out.

Two entirely different classes of methods allow the measurement of velocities without the step of identifying particles. The first is MRI, for which a useful variant utilizes a time-varying magnetic field as a probe. This allows the velocities of the MRI-active particles to be deconvolved from the response signal.[58] The second class of methods is all based on the scattering of waves, as described next.

One variant of the second class is to identify the phase shift of the scattered wave with radio detection and ranging (radar) systems because it is determined by the relative

distance between the scatterer and the observer. Radar methods can be implemented using electromagnetic wavelengths from visible light (LIDAR) through microwave and radio waves (>10 m) depending on the applications.[59] Tracers with a good contrast to the dielectric constant of the surrounding particles are then needed. For a moving target, a radar system compares the phase shift of the microwave being transmitted-to and scattered-from the object to get the position (moving target indicator radar). Alternatively, it uses the Doppler effect to obtain the velocity (Doppler radar).[60] The main advantage of radar particle tracking is the good time resolution. For continuous wave radar systems, the time resolution is only limited by the analog-to-digital converter. Methods for using this technique to obtain the displacement and consequently the instantaneous velocity of a tracer are described in an article of this Focus Issue.[37]

The other variant is to embrace the multiple-scattering limit, which leads to a loss of the information contained in the propagating wave.[36] Terahertz methods are not yet capable of measuring displacements or velocities. In the case of visible light and transparent grains, multiple scattering is unavoidable. Nevertheless, for illumination using coherent light, relative displacements can be obtained from the resulting speckle images arising from the interference of the numerous waves which have performed random walks in the system, a method called Diffusing-Wave Spectroscopy (DWS).[61,62] As with any interferometric method, minute relative displacements can be detected and typically deformations of the order of 10^{-5} can be obtained. In the case of back-scattering, most of the paths explore only a small volume in the vicinity of the illuminated plane. This means that spatially resolved displacement maps, with a resolution of typically a few bead diameters, can be obtained as a representation of the deformation field in a thin layer close to the plane of visualization. An example of a map of deformation obtained by this method is shown in Figure 2(c). These techniques are reviewed in an article of this Focus Issue.[35]

Finally, as discussed in the introduction, acoustic echo[42] or Doppler measurement[41] can be used to measure velocities in the limit of single scattering of the acoustic waves. The usefulness of such methods is rapidly limited by multiple scattering in granular piles.[63] Still, velocity fields have been recently obtained in dense suspensions using high-speed ultrasound imaging.[64]

IV. MEASURING INTER-PARTICLE FORCES

While rheological measurements[67] can provide the relationship between the bulk stress, strain, and strain-rate dynamics, these macroscopic tests do not provide insight into how the macroscopic behavior of a particulate material emerges from the interaction laws of the constituent particles. In particular, as can be seen from Fig. 3, the patterns of force transmission can be highly heterogeneous. To close this loop, it is necessary to track the internal (particle-scale) deformation of a sample, as discussed in Sections II and III. However, in order to link microscale information to macroscopic stresses, the only route is through a coarse grained formalism such as Irving-Kirkwood.[68] This formalism requires knowledge of
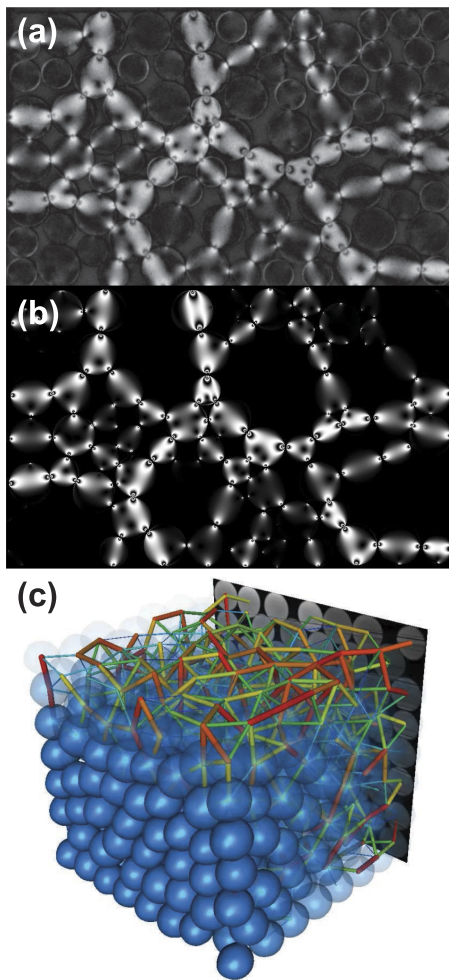
FIG. 3. (a) Image of force chains obtained using darkfield photoelastic measurements in the setup described in Ref. 65. The bright areas indicate the regions where contact forces modulate the photoelastic response of the disks. The quantitative extraction of contact forces works by finding the best set of contact forces to "fit" the bright pattern. (b) A computer generated fit to the data shown in (a). (c) Image of 3D interparticle forces obtained on frictionless hydrogel particles, from the experiment described in Ref. 66.

not only particle positions but also interparticle forces. Therefore measuring *forces between particles* becomes necessary to completely understand particulate materials.

The requirement to measure forces between particles in such particulate materials presents the experimentalist with great challenges. While Debye theory can predict heat capacities by making simplifying assumptions about the number of modes in a crystal lattice and a Lennard-Jones interaction potential suffices to predict the elastic behavior of most solids, granular materials require a more detailed model. First, the interaction laws between particles are generically dissipative, hysteretic, rate dependent, and not pairwise additive.[69,70] Second, the disordered nature eliminates the concept of linear response, such that "small deformation" analyses are of little use in understanding realistic materials.

Although it has been possible to obtain stress information at the boundary of a 3D system,[71,72] true understanding only comes if the spatiotemporal distribution of contact forces is also measured in the bulk of a particulate material, as it is often inhomogeneous and anisotropic. The complex distribution of

interparticle forces thus requires the experimentalist to measure not only the already-complex interaction forces between particles but also their spatial structure in generally opaque or at highly scattering media. The daunting task of performing complex force measurements in the bulk of a particulate material was steadily solved by the work of successive generations of physicists and engineers.

Photoelasticity, the change of the polarization state of light due to the stresses inside a birefringent material, has a century-old history[14,73,74] of measuring stress and strain distributions within both solids and granular materials. However, until the pioneering work of Behringer *et al.*[16] in which both normal and tangential interparticle forces were first measured, photoelastic studies were limited to the study of stress fields, and not the interparticle contact forces themselves. The quantitative photoelastic method has evolved tremendously and is now in advanced development across multiple labs around the world. These modern, quantitative methods are described here in a Focus Issue article,[24] as well as in the original theses.[75,76] A remaining challenge is that these methods are only suitable for Q2D studies if quantitative information is required.

Building on the development of conventional confocal microscopy tools, Brujic *et al.*[77] showed that it was possible to measure contact forces in the bulk of a 3D microemulsion (frictionless droplets) using fluorescent dyes. Since then, the emulsion measurement technique has grown to include a range of 3D force measurement techniques, including at larger granular length scales for frictionless particles.[66,78,79] In all cases, the central challenge is to measure the size of the contacts, which proceeds using similar techniques to those described in Section II. As described in a Focus Issue article,[34] such measurements are now possible while simultaneously performing mechanical tests under realistic strains. Due to the experimental and computational complexity of such studies, we present an overview of (partly published) experimental and computational methods used in the study of packings of hydrogel spheres. Similarly, X-ray tomography of non-transparent, frictional particles can provide normal forces for sufficiently soft particles.[80]

In addition, several other techniques not covered by the Focus Issue deserve mention since they provide contact force measurements for hard, frictional particles for which deformations are not directly observable. Using a combination of x-diffraction and X-ray tomography, Hurley *et al.*[81] have successfully measured inter-particle forces for a small sample of non-transparent particles under compression, and at the single-particle level. Chen *et al.*[82] have shown that it is possible to use two-photon excitation to make pressure measurements within single ruby particles, based on shifts in the fluorescence spectrum. It is an area of future research to use these methods to understand frictional responses through both the normal and tangential forces.

V. ACQUIRING OTHER PROPERTIES

The imaging of particles within granular media is done with an interest in measuring intensive properties such as the mean particle size, size distribution, packing density,

or structural measures. The analysis of large quantities of particles in order to calculate size distributions or packing structures is limited by the generic issues discussed in Sec. I. When further investigations do not require positions and shapes of the individual particle, investigation methods directly sensitive to such intensive material properties can be an effective alternative. We restrict the discussion to methods which are used in the statistical physics analysis of granular media. Methods that were developed for process technologies like sieving or elutriation are beyond the scope of this Focus Issue.

A. Mean size and size distribution

The fundamental task is to provide a measurement of the spatial extent of the particles in the system. This can be done by imaging a sufficiently large number of particles, with sufficient resolution, using any of the methods listed in Sec. II. However, it may take an excessively long time to image the ensemble and process the data (separating, identifying, and fitting each one) using one of the imaging methods optimized for opaque 3D materials.[40] Specialized automated setups can image and process tens of thousands of particles in seconds, if disassembly of the sample and *ex situ* characterization of the particles are possible.[83] Particle sizes between a few micrometers and a few millimeters can be resolved by imaging.

An alternative to imaging is small-angle light scattering. This method relies on the multiple-scattering of light intensity by particles in a well-collimated light beam. The relative intensity changes are sensitive to the particle size, but only when the particles are not much larger than the wavelength of the light used. Consequently, specialized instruments are required to resolve the intensity changes by such scattering.[84] Recently, terahertz radiation with 87 μm wavelength has been applied to macroscopic granular particles, which has lowered the instrumental demands to a manageable range.[85]

In general, scattering methods can be applied to any particle material. Mean particle size and particle size distributions can be determined from single measurements on particle ensembles. Nonetheless, the samples must be disassembled and heavily diluted in order to reach the independent-scattering regime. In practice, this leads to measurement times no faster than the automated imaging setups, and only radii of equivalent spheres are obtained.[84] Particles sizes between hundred nanometers and roughly a millimeter can be analyzed with scattering.

B. Packing density and packing structure

For some imaging methods which are sensitive to an extensive property of the sample, it is possible to use them in a way that reports the average packing density. For example, in X-ray radiography the intensity decreases exponentially with the number of particles in the beam path. Other examples include index matching and MRI (compare Sec. II). For index-matched and fluorescent-dyed samples, the intensity of the signal is proportional to the number of particles containing fluorescence markers (or inversely proportional, if the liquid contains the fluorescence molecules). For MRI, the signal is proportional to the number of particles containing NMR-active liquids. This means that these methods can switch to a mode which records packing density, even when the resolution would be insufficient to resolve individual particles. In each case, the signal is normalized by a sample volume to obtain the packing density. These techniques have allowed X-ray radiograms to be used to study density variations in flowing sand,[86,87] dilatancy during fast shear,[54,88,89] or the formation of a jet after a sphere impact into a granular medium.[90,91] MRI has been further used to quantify the evolution of the local particle density, e.g., in colloid transport,[92] during sedimentation,[93–96] or in smooth granular shear[97] (see Fig. 4).

Conventionally, methods that are directly sensitive to the packing structure rely on measuring scattering patterns. The scattering pattern is sensitive to the packing structure only for samples which exhibit single scattering of a certain wave.[98] This is frequently the case for colloidal and atomic systems and light or X-ray scattering, but packing density and scattering efficiency of granular media are too large for this technique to work.[36] One novel approach which moves the field towards direct structure sensitivity is presented in this Focus Issue. In Ref. 36, we show that the spectroscopic transmission of
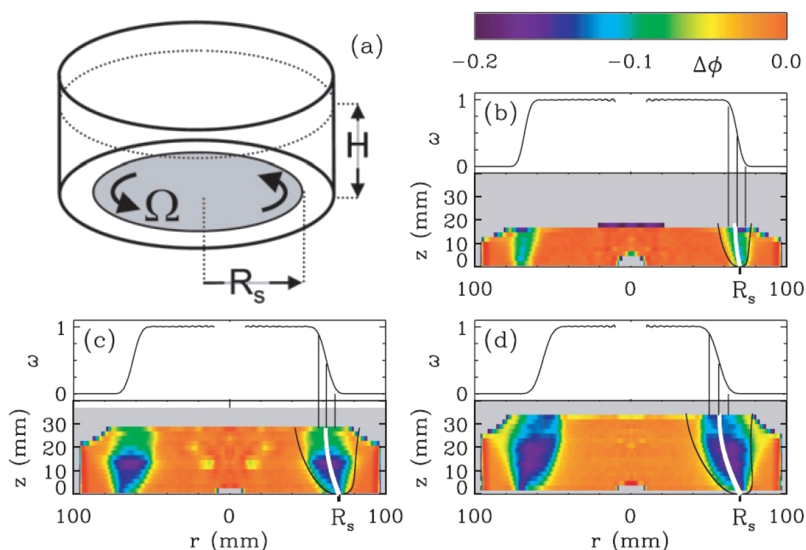

FIG. 4. Visualization of shear dilatancy by means of MR imaging. In this study, a disk in the bottom of a cylindrical container filled with poppy seeds is continuously rotated until shear dilatancy reaches a stationary value (a). The drop of packing fraction $\Delta\Phi$ was determined from MRI intensity profiles. Subfigures ((b)-(d)) show the dilatancy profiles for different filling heights (bottom) together with the profiles of the rotation velocity at the granular surface (top). The shear zone edges are indicated by black lines. Reprinted with permission from Sakaie *et al.*, EPL **84**, 38001 (2008). Copyright 2008 IOP Publishing.

terahertz radiation through granular materials reveals the position of the structure factor peak (the strongest correlation length in the sample). This approach requires that the particle diameter is within the spectral range of the wavelengths used, and that the particle material does not absorb the radiation too much.

C. Particle contact stability

The local stability and the statistics of particle contacts in consolidated packings can be qualitatively probed with sound. Sound waves propagate within granular media along the force chains formed by the discrete particle contacts[99] and the velocity of the acoustic wave gives indication on the structure of the granular pile.[100] Scattering and dissipation of the wave occurs at each contact, leading to diffusive transmission of sound and high attenuation. Simulations have shown that the scattering losses are sensitive to the degree of disorder in the contact network.[101] Intensity losses by dissipation are sensitive to friction at the contacts.[43] Time-of-flight measurements allow separating the contributions to attenuation by scattering and dissipation.[43] The momentum and kinetic energy associated with the sound wave are often sufficient to induce rearrangements in granular media with low confining pressures, which can itself be used to probe rigidity and local unjamming in granular media.[102,103] Further investigations of the individual contributions of dissipation, scattering, order, and mechanical impact by sound waves might lead to new methods to probe statistics of the contact network in granular media without having to image individual contacts.

VI. CONCLUSION AND OUTLOOK

This Focus Issue reviews methods for acquiring microscopic particle properties and for connecting them to the macroscopic physics of granular media. A variety of methods are presented, utilizing electromagnetic waves ranging from γ-rays to radio waves. These methods provide information in the form of images, scattering, tomographic reconstruction, and the tracking of phase shifts. Each approach and probe has specific demands on sample material, instrumental investments, and computational efforts and offers different sensitivities and spatiotemporal resolutions. This introductory article aims to assist the reader in selecting the most appropriate techniques for their particular research.

To consider the success of these methods, it is only necessary to return to the question raised in the initial paragraph of this paper: how do individual grains contribute to the intermittent flow of sand while walking on the beach? In spite of the latest advances in methods presented here, a comprehensive answer to such a question remains beyond reach of even the most advanced contemporary techniques.

As such, the methods presented here demand future developments to improve both quality and precision. The continued closing of the gap between the lab and beach can be deduced from the remaining limitations discussed in this paper. We expect most beneficial improvements will arise in the following area: (1) efficient tracking of both the translation (easier) and rotation (harder) of particles; (2) techniques for

investigating packings of irregular particles; (3) reconstructing 3D force distributions; (4) improved computational capability and efficiency. In particular, the simultaneous tracking of rotational motion of many particles is still in its infancy. Working with irregular particles may move studies away from the "spherical cow" paradigm towards more realistic sand grains. The development of low-cost 3D printers is already fostering rapid interest in more-complex shaped particles.[104] Approaches to the reconstruction of forces in 3D packings of hard particles have been demonstrated by fluorescence imaging and X-ray diffraction.

Item (4) is particularly noteworthy, as it might seem that Moore's law will take care of this problem without interference from granular scientists. However, each of the other three items on the list significantly increases the amount of data to be handled. Tracking rotation and translation at the same time doubles the amount of data per particle, working with irregular particles requires better shape detection algorithms and keeping track of more descriptive variables, and the reconstruction of 3D force distributions requires new detection and fitting algorithms as well as an increase in the number of parameters (contacts and force vectors) stored in the final dataset. As the spatiotemporal resolution of tomographic methods improves, the amount of data grows as a cubic function. As such, data science initiatives and algorithmic advances will be key to the success of the field.

[1]G. Greenberg, *A Grain of Sand: Nature's Secret Wonder* (Voyageur Press, St. Paul, MN, 2008).

[2]J. Duran, *Sands, Powders and Grains an Introduction to the Physics of Granular Materials*, 1st ed. (Springer-Verlag, New York, 2000).

[3]J. Geng, D. Howell, E. Longhi, R. P. Behringer, G. Reydellet, L. Vanel, E. Clément, and S. Luding, "Footprints in sand: The response of a granular material to local perturbations," Phys. Rev. Lett. **87**, 035506 (2001).

[4]S. Herminghaus, *Wet Granular Matter: A Truly Complex Fluid* (World Scientific, Singapore, 2013).

[5]F. Charru, B. Andreotti, and P. Claudin, "Sand ripples and dunes," Annu. Rev. Fluid Mech. **45**, 469–493 (2013).

[6]J. T. Jenkins and S. B. Savage, "A theory for the rapid flow of identical, smooth, nearly elastic, spherical particles," J. Fluid Mech. **130**, 187 (1983).

[7]I. Goldhirsch, "Rapid granular flows," Annu. Rev. Fluid Mech. **35**, 267 (2003).

[8]G. D. R. MiDi, "On dense granular flows," Eur. Phys. J. E **14**, 341 (2004).

[9]A. J. Liu and S. R. Nagel, "The jamming transition and the marginally jammed solid," Annu. Rev. Condens. Matter Phys. **1**, 347 (2010).

[10]I. S. Aranson and L. S. Tsimring, *Granular Patterns* (Oxford University Press, 2009).

[11]S. Luding, "Granular materials under vibration: Simulations of rotating spheres," Phys. Rev. E **52**, 4442 (1995).

[12]N. Brilliantov and T. Pöschel, *Kinetic Theory of Granular Gases* (Oxford University Press, Oxford, New York, 2004).

[13]T. Müller and K. Huang, "Influence of the liquid film thickness on the coefficient of restitution for wet particles," Phys. Rev. E **93**, 042904 (2016).

[14]P. Dantu, "Contribution l'étude mécanique et géométrique des milieux pulvérulents," in *Proceedings of the Fourth International Conference on Soil Mechanics and Foundation Engineering* (Butterworths Scientific Publications, London, 1957), pp. 144–148.

[15]J. Geng, E. Longhi, R. Behringer, and D. Howell, "Memory in two-dimensional heap experiments," Phys. Rev. E **64**, 060301 (2001).

[16]T. S. Majmudar and R. P. Behringer, "Contact force measurements and stress-induced anisotropy in granular materials," Nature **435**, 1079–1082 (2005).

[17]F. Radjai, D. E. Wolf, M. Jean, and J.-J. Moreau, "Bimodal character of stress transmission in granular packings," Phys. Rev. Lett. **80**, 61–64 (1998).

[18]F. Radjai and S. Roux, "Turbulentlike fluctuations in quasistatic flow of granular media," Phys. Rev. Lett. **89**, 064302 (2002).

[19]P. Schall and M. van Hecke, "Shear bands in matter with granularity," Annu. Rev. Fluid Mech. **42**, 67–88 (2010).

[20]K. Nichol, A. Zanin, R. Bastien, E. Wandersman, and M. van Hecke, "Flow-induced agitations create a granular fluid," Phys. Rev. Lett. **104**, 078302 (2010).

[21]K. A. Reddy, Y. Forterre, and O. Pouliquen, "Evidence of mechanically activated processes in slow granular flows," Phys. Rev. Lett. **106**, 108301 (2011).

[22]P. M. Reis, R. A. Ingale, and M. D. Shattuck, "Crystallization of a quasi-two-dimensional granular fluid," Phys. Rev. Lett. **96**, 258001 (2006).

[23]K. Huang, "1/f noise on the brink of wet granular melting," New J. Phys. **17**, 083055 (2015).

[24]K. E. Daniels, J. E. Kollmer, and J. G. Puckett, "Photoelastic force measurements in granular materials," Rev. Sci. Instrum. **88**, 051808 (2017).

[25]W. Zhang, K. E. Thompson, A. H. Reed, and L. Beenken, "Relationship between packing structure and porosity in fixed beds of equilateral cylindrical particles," Chem. Eng. Sci. **61**, 8060–8074 (2006).

[26]A. V. Orpe and A. Kudrolli, "Velocity correlations in dense granular flows observed with internal imaging," Phys. Rev. Lett. **98**, 238001 (2007).

[27]M. Jerkins, M. Schröter, H. L. Swinney, T. J. Senden, M. Saadatfar, and T. Aste, "Onset of mechanical stability in random packings of frictional spheres," Phys. Rev. Lett. **101**, 018301 (2008).

[28]K. W. Desmond and E. R. Weeks, "Random close packing of disks and spheres in confined geometries," Phys. Rev. E **80**, 051305 (2009).

[29]S. G. K. Tennakoon, L. Kondic, and R. P. Behringer, "Onset of flow in a horizontally vibrated granular bed: Convection by horizontal shearing," EPL **45**, 470 (1999).

[30]A. Raihane, O. Bonnefoy, J. M. Chaix, J. L. Gelet, and G. Thomas, "Analysis of the densification of a vibrated sand packing," Powder Technol. **208**, 289–295 (2011).

[31]R. J. Adrian and J. Westerweel, *Particle Image Velocimetry* (Cambridge University Press, 2011), Vol. 30.

[32]M. Raffel, C. Willert, S. Wereley, and J. Kompenhans, *Particle Image Velocimetry*, Experimental Fluid Mechanics (Springer, Berlin, 2007), Vol. 10, pp. 978–983.

[33]C. Cierpka and C. Kähler, "Particle imaging techniques for volumetric three-component ($_3$D$_3$C) velocity measurements in microfluidics," J. Visualization **15**, 1–31 (2012).

[34]J. A. Dijksman, N. Brodu, and R. P. Behringer, "Refractive index matched scanning and detection of soft particles," Rev. Sci. Instrum. **88**, 051807 (2017).

[35]A. Amon, A. Mikhailovskaya, and J. Crassous, "Spatially-resolved measurements of micro-deformations in granular materials using DWS," Rev. Sci. Instrum. **88**, 051804 (2017).

[36]P. Born and K. Holldack, "Analysis of granular packing structure by scattering of THz radiation," Rev. Sci. Instrum. **88**, 051802 (2017).

[37]F. Ott, S. Herminghaus, and K. Huang, "Radar for tracer particles," Rev. Sci. Instrum. **88**, 051801 (2017).

[38]D. Parker, "Positron emission particle tracking and its application to granular media," Rev. Sci. Instrum. **88**, 051803 (2017).

[39]R. Stannarius, "Magnetic resonance imaging of granular materials," Rev. Sci. Instrum. **88**, 051806 (2017).

[40]S. Weis and M. Schröter, "Analyzing x-ray tomographies of granular packings," Rev. Sci. Instrum. **88**, 051809 (2017).

[41]Y. Takeda, "Velocity profile measurement by ultrasound doppler shift method," Int. J. Heat Fluid Flow **7**, 313–318 (1986).

[42]S. Manneville, L. Bcu, and A. Colin, "High-frequency ultrasonic speckle velocimetry in sheared complex fluids," Eur. Phys. J. Appl. Phys. **28**, 361–373 (2004).

[43]X. Jia, "Codalike multiple scattering of elastic waves in dense granular media," Phys. Rev. Lett. **93**, 154303 (2004).

[44]See https://www.youtube.com/watch?v=76Z1Bbj7CtQ for an animated version of Fig. 1(b) (2011).

[45]J. Bernal and J. Mason, "Packing of spheres: Co-ordination of randomly packed spheres," Nature **188**, 910–911 (1960).

[46]D. Fenistein, J.-W. van de Meent, and M. van Hecke, "Universal and wide shear zones in granular bulk flow," Phys. Rev. Lett. **92**, 094301 (2004).

[47]S. Wiederseiner, N. Andreini, G. Epely-Chauvin, and C. Ancey, "Refractive-index and density matching in concentrated particle suspensions: A review," Exp. Fluids **50**, 1183–1206 (2011).

[48]J. A. Dijksman, F. Rietz, K. A. Lorincz, M. van Hecke, and W. Losert, "Refractive index matched scanning of dense granular materials," Rev. Sci. Instrum. **83**, 011301 (2012).

[49]T. M. Buzug, *Computed Tomography—From Photon Statistics to Modern Cone-Beam CT* (Springer, 2008).

[50]A. G. Athanassiadis, P. J. L. Rivière, E. Sidky, C. Pelizzari, X. Pan, and H. M. Jaeger, "X-ray tomography system to investigate granular materials during mechanical loading," Rev. Sci. Instrum. **85**, 083708 (2014).

[51]I. Vlahinić, E. Andò, G. Viggiani, and J. E. Andrade, "Towards a more accurate characterization of granular media: Extracting quantitative descriptors from tomographic images," Granular Matter **16**, 9–21 (2014).

[52]H. T. Xu, A. P. Reeves, and M. Y. Louge, "Measurement errors in the mean and fluctuation velocities of spherical grains from a computer analysis of digital images," Rev. Sci. Instrum. **75**, 811–819 (2004).

[53]J. R. Agudo, G. Luzi, J. Han, M. Hwang, J. Lee, and A. Wierschem, "Detection of particle motion using image processing with particular emphasis on rolling motion," Rev. Sci. Instrum. **88**, 051805 (2017).

[54]N. Uhlmann, T. Pöschel, and M. Schröter, "Beam hardening in X-ray radiography" (unpublished).

[55]N. B. Tuyen and N.-S. Cheng, "A single-camera technique for simultaneous measurement of large solid particles transported in rapid shallow channel flows," Exp. Fluids **53**, 1269–1287 (2012).

[56]C. Cierpka, B. Lütke, and C. J. Kähler, "Higher order multi-frame particle tracking velocimetry," Exp. Fluids **54**, 1533 (2013).

[57]Q. Gao, H. Wang, and G. Shen, "Review on development of volumetric particle image velocimetry," Chin. Sci. Bull. **58**, 4541–4556 (2013).

[58]E. Fukushima, "Nuclear magnetic resonance as a tool to study flow," Annu. Rev. Fluid Mech. **31**, 95 (1999).

[59]M. I. Skolnik, *Introduction to Radar Systems*, 3rd ed. (McGraw Hill, Boston, 2001).

[60]*Radar Handbook*, 3rd ed., edited by M. I. Skolnik (McGraw-Hill Education, New York, 2008).

[61]D. A. Weitz and D. J. Pine, "Diffusing-wave spectroscopy," in *Dynamic Light Scattering: The Method and Some Applications* (Oxford University Press, 1993).

[62]V. Viasnoff, F. Lequeux, and D. J. Pine, "Multispeckle diffusing-wave spectroscopy: A tool to study slow relaxation and time-dependent dynamics," Rev. Sci. Instrum. **73**, 2336 (2002).

[63]X. Jia, C. Caroli, and B. Velicky, "Ultrasound propagation in externally stressed granular media," Phys. Rev. Lett. **82**, 1863–1866 (1999).

[64]E. Han, I. R. Peters, and H. M. Jaeger, "High-speed ultrasound imaging in dense suspensions reveals impact-activated solidification due to dynamic shear jamming," Nat. Commun. **7**, 12243 (2016).

[65]J. Ren, J. A. Dijksman, and R. P. Behringer, "Reynolds pressure and relaxation in a sheared granular system," Phys. Rev. Lett. **110**, 018302 (2013).

[66]N. Brodu, J. A. Dijksman, and R. P. Behringer, "Spanning the scales of granular materials through microscopic force imaging," Nat. Commun. **6**, 6361 (2015).

[67]P. Coussot, *Rheometry of Pastes, Suspensions and Granular Materials* (Wiley, 2005).

[68]J. H. Irving and J. G. Kirkwood, "The statistical mechanical theory of transport processes. IV. The equations of hydrodynamics," J. Chem. Phys. **18**, 817–829 (1950).

[69]N. Brodu, J. A. Dijksman, and R. P. Behringer, "Multiple-contact discrete-element model for simulating dense granular media," Phys. Rev. E **91**, 032201 (2015).

[70]R. Höhler and S. Cohen-Addad, "Many-body interactions in soft jammed materials," Soft Matter **13**, 1371 (2017).

[71]J. M. Erikson, N. W. Mueggenburg, H. M. Jaeger, and S. R. Nagel, "Force distributions in three-dimensional compressible granular packs," Phys. Rev. E **66**, 040301 (2002).

[72]D. M. Mueth, H. M. Jaeger, and S. R. Nagel, "Force distribution in a granular medium," Phys. Rev. E **57**, 3164–3169 (1998).

[73]J. P. D. Hartog, "Book review: Photoleasticity," Science **92**, 382 (1940).

[74]C. H. Liu, S. R. Nagel, D. A. Schecter, S. N. Coppersmith, S. Majumdar, O. Narayan, and T. A. Witten, "Force fluctuations in bead packs," Science **269**, 513–515 (1995).

[75]D. Howell, "Stress distributions and fluctuations in static and quasi-static granular systems," Ph.D. thesis, Duke University, 1999.

[76]T. Majmudar, "Experimental studies of two-dimensional granular systems using grain-scale contact force measurements," Ph.D. thesis, Duke University, 2006.

[77]J. Brujic, S. Edwards, I. Hopkinson, and H. Makse, "Measuring the distribution of interdroplet forces in a compressed emulsion system," Physica A **327**, 201–212 (2003).

[78]J. Zhou, S. Long, Q. Wang, and A. D. Dinsmore, Science **312**, 1631–1633 (2006).

[79]K. W. Desmond, P. J. Young, D. Chen, and E. R. Weeks, "Experimental study of forces between quasi-two-dimensional emulsion droplets near jamming," Soft Matter **9**, 3424 (2013).

[80]M. Saadatfar, A. P. Sheppard, T. J. Senden, and A. J. Kabla, "Mapping forces in a 3D elastic assembly of grains," J. Mech. Phys. Solids **60**, 55–66 (2012).

[81]R. Hurley, S. Hall, J. Andrade, and J. Wright, "Quantifying interparticle forces and heterogeneity in 3D granular materials," Phys. Rev. Lett. **117**, 098005 (2016).

[82]Y. Chen, A. Best, H.-J. Butt, R. Boehler, T. Haschke, and W. Wiechert, "Pressure distribution in a mechanical microcontact," Appl. Phys. Lett. **88**, 234101 (2006).

[83]W. Yu and B. C. Hancock, "Evaluation of dynamic image analysis for characterizing pharmaceutical excipient particles," Int. J. Pharm. **361**(1-2), 150–157 (2008).

[84]R. Xu, *Particle Technology Series* (Kluwer Academic Press, Dordrecht, 2000).

[85]P. Born, N. Rothbart, M. Sperl, and H.-W. Hübers, "Granular structure determined by terahertz scattering," EPL **106**, 48006 (2014).

[86]R. L. Michalowski, "Flow of granular material through a plane hopper," Powder Technol. **39**, 29–40 (1984).

[87]G. W. Baxter, R. P. Behringer, T. Fagert, and G. A. Johnson, "Pattern formation in flowing sand," Phys. Rev. Lett. **62**, 2825–2828 (1989).

[88]J. Desrues, "Tracking strain localization in geomaterials using computerized tomography," in *X-ray CT for Geomaterials*, edited by J. Otani and Y. Obara (Swets & Zeitlinger, 2004), pp. 15–41.

[89]A. J. Kabla and T. J. Senden, "Dilatancy in slow granular flows," Phys. Rev. Lett. **102**, 228301 (2009).

[90]J. R. Royer, E. I. Corwin, A. Flior, M.-L. Cordero, M. L. Rivers, P. J. Eng, and H. M. Jaeger, "Formation of granular jets observed by high-speed X-ray radiography," Nat. Phys. **1**, 164–167 (2005).

[91]T. Homan, R. Mudde, D. Lohse, and D. van der Meer, "High-speed X-ray imaging of a ball impacting on loose sand," J. Fluid Mech. **777**, 690–706 (2015).

[92]T. Baumann and C. J. Werth, "Visualization of colloid transport through heterogeneous porous media using magnetic resonance imaging," Colloids Surf., A **265**, 2 (2005).

[93]G. Ovarlez, F. Bertrand, P. Coussot, and X. Chateau, "Shear-induced sedimentation in yield stress fluids," J. Non-Newtonian Fluid Mech. **177-178**, 19–28 (2012).

[94]E. V. Morozov, O. V. Shabanova, and O. V. Falaleev, "MRI comparative study of container geometry impact on the PMMA spheres sedimentation," Appl. Magn. Res. **44**, 619–636 (2013).

[95]Z. Wuxin, J. Martins, P. Saveyn, R. Govoreanu, K. Verbruggen, T. Arien, A. Verliefde, and P. Van der Meeren, "Sedimentation and resuspendability evaluation of pharmaceutical suspensions by low-field one dimensional pulsed field gradient NMR profilometry," Pharm. Dev. Technol. **18**, 787–797 (2013).

[96]R. Harich, T. W. Blythe, M. Hermes, E. Zaccarelli, A. J. Sederman, L. F. Gladden, and W. C. K. Poon, "Gravitational collapse of depletion-induced colloidal gels," Soft Matter **12**, 4300–4308 (2016).

[97]K. Sakaie, D. Fenistein, T. J. Carroll, M. van Hecke, and P. Umbanhowar, "MR imaging of Reynolds dilatancy in the bulk of smooth granular flows," EPL **84**, 38001 (2008).

[98]L. A. Feigin and D. I. Svergun, *Structure Analysis by Small-Angle X-ray and Neutron Scattering* (Plenum Press, New York, 2000).

[99]E. T. Owens and K. E. Daniels, "Sound propagation and force chains in granular materials," EPL **94**, 54005 (2011).

[100]S. Lherminier, R. Planet, G. Simon, L. Vanel, and O. Ramos, "Revealing the structure of a granular medium through ballistic sound propagation," Phys. Rev. Lett. **113**, 098001 (2014).

[101]O. Mouraille and S. Luding, "Sound wave propagation in weakly polydisperse granular materials," Ultrasonics **48**, 498–505 (2008).

[102]S. van den Wildenberg, Y. Yang, and X. Jia, "Probing the effect of particle shape on the rigidity of jammed granular solids with sound speed measurements," Granular Matter **17**, 419–426 (2015).

[103]P. Lidon, N. Taberlet, and S. Manneville, "Grains unchained: Local fluidization of a granular packing by focused ultrasound," Soft Matter **12**, 2315–2324 (2016).

[104]H. M. Jaeger, "Celebrating soft matter's 10th anniversary: Toward jamming by design," Soft Matter **11**, 12–27 (2015).